Composites Part B 184 (2020) 107625

Contents lists available at ScienceDirect

Composites Part B

journal homepage: www.elsevier.com/locate/compositesb

Multifunctional performance of carbon nanotubes and graphene nanoplatelets reinforced PEEK composites enabled via FFF additive manufacturing

M.F. Arif [a,f], H. Alhashmi [a], K.M. Varadarajan [b,c], Joseph H. Koo [d], A.J. Hart [e], S. Kumar [a,*]

[a] Department of Mechanical Engineering, Khalifa University of Science and Technology, Masdar Campus, Masdar City, P.O. Box 54224, Abu Dhabi, United Arab Emirates
[b] Department of Orthopaedic Surgery, Harris Orthopaedics Laboratory, Massachusetts General Hospital, 55 Fruit St, Boston, USA
[c] Department of Orthopaedic Surgery, Harvard Medical School, A-111, 25 Shattuck Street, Boston, USA
[d] Department of Mechanical Engineering, University of Texas at Austin, Austin, TX, 78712, USA
[e] Department of Mechanical Engineering, Massachusetts Institute of Technology, Cambridge, MA, 02139, USA
[f] Department of Materials Engineering, Institut Teknologi Sumatera, South Lampung, 35365, Indonesia

ARTICLE INFO

Keywords:
PEEK nanocomposites
Fused filament fabrication (FFF)
Carbon nanostructures
Coefficient of thermal expansion (CTE)
Wear

ABSTRACT

The study is focused on multifunctional performance of carbon nanotubes (CNT) and Graphene nanoplatelets (GNP) reinforced PEEK composites enabled via fused filament fabrication (FFF) additive manufacturing (AM) utilizing in-house nanoengineered filaments. Thermo-physical, mechanical and wear characteristics of electro-conductive PEEK nanocomposites are reported. The coefficient of thermal expansion (CTE) is found to decrease by 26% and 18% with the incorporation of 5 wt% GNP and 3 wt% CNT into PEEK polymer, respectively. The decrease in CTE provides better dimensional stability to resulting nanocomposite structures. Due to uniform dispersion of CNT and GNP in the PEEK matrix, the crystallization temperature and degree of crystallinity are both increased. The 3D printed PEEK nanocomposites reveal interfacial voids between the beads and intra-bead pores and thus exhibit lower density compared to that of the 3D printed neat PEEK. Young's and storage moduli are found to increase by 20% and 66% for 3 wt% CNT loading and by 23% and 72% for 5 wt% GNP loading respectively. However, the PEEK nanocomposites exhibit similar tensile strength to that of neat PEEK. The co-efficient of friction obtained from fretting wear tests is found to decrease by 67% and 56% for 1 wt% CNT and 3 wt% GNP loaded PEEK nanocomposites, respectively and the decrease is attributed to reduced hardness and increased porosity. Multifunctional performance of carbon nanostructures reinforced AM-enabled PEEK composites demonstrated here makes them suitable for a range of applications such as orthopedics, oil and gas, automotive, electronics and space.

1. Introduction

Additive manufacturing (AM) enables fabrication of complex geometries through layer-by-layer formation and is rapidly advancing towards new materials and applications [1,2]. AM offers user friendly and low-cost fabrication route that provides greater flexibility to locally design the material architecture in three-dimensions [3–6]. Fused filament fabrication (FFF), also known as fused deposition modeling (FDM) is the most popular AM technique for thermoplastics due to its relative simplicity and low-cost. In FFF process, the filament feedstock is fed into a heated nozzle where the polymer is fused and subsequently deposited on to a heated plate to form a 3D part, following a predefined 3D slicing pattern.

Despite abundant availability of FFF machines, only a few are suitable for 3D printing high performance polymers, such as polyether ether ketone (PEEK), polyetherimide (PEI), etc., as they process at high temperature. These polymers exhibit superior mechanical properties as well as high thermal and chemical resistance [7]. Among the high performance polymers, PEEK, a semi-crystalline polymer is suitable for many engineering applications, such as biomedical implants, due to its biocompatibility, corrosion resistance, radiopacity, excellent fatigue and wear resistance [8]. PEEK is also utilized for space applications as

* Corresponding author.
E-mail address: s.kumar@eng.oxon.org (S. Kumar).

https://doi.org/10.1016/j.compositesb.2019.107625
Received 10 June 2019; Received in revised form 21 August 2019; Accepted 25 November 2019
Available online 27 November 2019

PEEK has low outgassing property and lightweight relative to metals [9]. PEEK and PEEK composites are also used in oil and gas industries for gaskets and seals. These components interact with potentially harsh environments, such as extreme temperatures and high pressures, corrosive fluids and gases, lubricating oils and solvents [10]. The drawbacks of PEEK are higher cost (compared to other commodity thermoplastics), high processing temperature (above 350 °C) and the processing difficulties associated with its semi-crystallinity. FFF technique has been successfully utilized to fabricate PEEK [11–17]. The expensive selective laser sintering (SLS) AM technique has also been utilized to fabricate PEEK [18].

Precursor materials (e.g., filament, mixed photo-resin) containing micro and/or nano-fillers, such as carbon fiber [19,20], carbon black [21], GNP [22,23], CNT [24], montmorillonite [25], stainless steel, bronze and copper powders [26,27], glass microspheres and nanoclay [28], and wood flour [27] are increasingly being developed to realize AM-enabled composites. The main idea is to harness the synergistic effects of their constituents and their tailorable microstructure to realize lightweight composites with superior mechanical, electrical, thermal and coefficient of thermal expansion (CTE) properties. Strong parts with low CTE are desirable to ensure dimensional stability. However, typical polymers possess high CTE. It was found that the PEEK CTE can be reduced by the incorporation of low CTE and high thermal conductivity Al_2O_3 particles [29]. Additionally, polymers reinforced with electrically conductive nanofibers, such as GNP and/or CNT have also been explored for their functional performance, such as for temperature, strain and damage-sensing [30–34]. Stepashkin et al. [19]. reported that Carbon fiber-reinforced PEEK composites fabricated by FFF process exhibit 25–30% lower thermal conductivity than cast CF/PEEK composites. Anisotropy of thermal properties was observed, as the short carbon fibers get oriented along the FFF deposition path. Berretta et al. [35]. fabricated PEEK nanocomposites reinforced with 1 wt% and 5 wt% CNT by FFF process and found that the incorporation of CNT into the PEEK matrix, does not influence the mechanical performance of the PEEK nanocomposites. Gonçalves et al. [36]. fabricated PEEK nanocomposite filaments reinforced with CNT/GNP. The resulting nanocomposite filaments exhibit electrical conductivity between 1.5 and 13.1 S/m.

The reinforcement of PEEK with CNT and GNP also influences the tribological characteristics of resulting PEEK composites. For example, addition of GNP into PEEK was found to reduce the coefficient of friction by 38% of the nanocomposite due to the lubrication action of GNP [37]. In another study, incorporation of CNT into PEEK matrix was found to result in a ~24% reduction in the friction compared to the neat PEEK [38]. The microscale wear (known as fretting wear) test is usually performed to assess the tribological performance of PEEK and PEEK nanocomposites used especially for artificial joints in orthopedics and mechanical bearings [38]. Artificial joints, experience microscale oscillatory movements between the mating surfaces [39–41]. Fretting wear analysis can predict the possibility of loosening of the implant due to wear at the joints [42].

Either most of the aforementioned studies focused on conventional fabrication of PEEK nanocomposites or 3D printed composites utilizing filaments produced by third party. In this study, we developed carbon nanostructures (CNT and GNP) engineered PEEK filaments and fabricated electro-conductive PEEK nanocomposites enabled via FFF AM. We investigated the effect of GNP (3 and 5 wt%) and CNT (1 and 3 wt%) on multifunctional properties of PEEK filaments and their corresponding FFF-PEEK nanocomposites. The melting temperature, degree of crystallinity, and density of the filament feedstocks are analyzed. The density, CTE, tensile properties, dynamic mechanical properties, and surface morphology of the PEEK nanocomposites are then investigated. The Fretting wear performance of PEEK, CNT/PEEK and GNP/PEEK composites is assessed against stainless steel counter body. The multifunctional performance of 3D printed GNP/PEEK and CNT/PEEK electro-conductive composites demonstrated in this study signify their potential for several structural and functional applications.

2. Materials and methods

2.1. Materials

The KetaSpire® KT-880 high flow, injection molding grade PEEK (Solvay Specialty Polymers, www.solvay.com) was used as the matrix. This is a medical grade PEEK supplied in a lubricated pellet form, with 0.01% calcium stearate lubricant to aid the pellet flow through plasticisation screws. Two carbon nanostructures were used as nanoreinforcements: Graphistrength™ C100 multiwall CNT (Arkema, Lacq, France; www.graphistrength.com) and Grafmax HC 11 GNP (Nacional de Grafite, San Paulo, Brazil; www.grafite.com). Graphistrength® C100 MWCNT is a black powder with an apparent density of 50–150 kg/m^3, mean agglomerate size of 200–500 μm, C content greater than 90 wt%, mean number of walls of 5–15, an outer mean diameter of 10–15 nm, and length about 0.1–10 μm [43]. Grafmax® HC 11 GNP is a black powder with a C content great than 99.5 wt%. It has a $D_{32} = 6.99$ μm, and a platelet thickness from about 0.34 to 100 nm [43].

2.2. Filament fabrication

To manufacture filament of an appropriate size for use in FFF machines, a filament extrusion system consisting of a twin-screw extruder, water bath, a customized filament puller, and a winding device was setup as shown in Fig. S1. To achieve precise speed control, the filament puller consists of a potentiometer, an Arduino controller, and a stepper motor. For extrusion, a Thermo Scientific Process 11 parallel co-rotating twin-screw extruder was used to melt compound the CNT/PEEK (1 and 3 wt%) and GNP/PEEK (3 and 5 wt%). To ensure a homogenous dispersion, formulations with varying concentrations were stir mixed prior to melt compounding. It is interesting to note that the GNP/PEEK compound with 3–5 wt% GNP and CNT/PEEK compound with 1 wt% CNT showed good melt processability, whereas CNT/PEEK compound with 3 wt% CNT was very viscous. Viscous compound, due to its unstable melt flow, makes the filament diameter non-uniform. This in turn influences the printability of filaments and the properties of printed parts. The weight fraction of carbon nanostructures is chosen such that they form electrically percolating network in the resulting nanocomposite (electrical conductivity $\sigma = 9.1 \times 10^{-7}$ S/cm for 1 wt% CNT) but still small enough for the nanocomposite to remain biocompatible.

2.3. FFF fabrication

Indmatec (Apium) HPP 155 3D printer was used to fabricate the specimens. Neat and nanoengineered PEEK filaments with an average diameter of 1.75 mm were used as feedstock. The deposition path and FFF parameters were defined using Simplify3D (a 3D printing slicer software). Nozzle movement speed of 1000 mm/min, nozzle temperature of 390 °C, bed temperature of 100 °C, layer height of 0.1 mm, extrusion width of 0.48 mm, and infill density of 100% were selected as the FFF process parameters. The specimens were fabricated in two different print orientations, namely, horizontal and vertical, as described in Fig. 1. One specimen of horizontal print orientation, and four specimens of vertical print orientation were produced per fabrication cycle. Different number of specimens were selected to ensure a successful fabrication, as discussed in our recent work [17].

2.4. Characterization

Differential scanning calorimetry (DSC) measurements (Netzsch) were performed under nitrogen atmosphere to study the melting and crystallization behavior of neat PEEK and in-house nanoengineered PEEK filaments. The samples were heated from 30 °C to 430 °C at a heating rate of 10 °C/min and then maintained isothermally at 430 °C for 5 min before cooling the samples to 30 °C at the same rate of 10 °C/min. Subsequently after soaking isothermally for 5 min at 30 °C, the

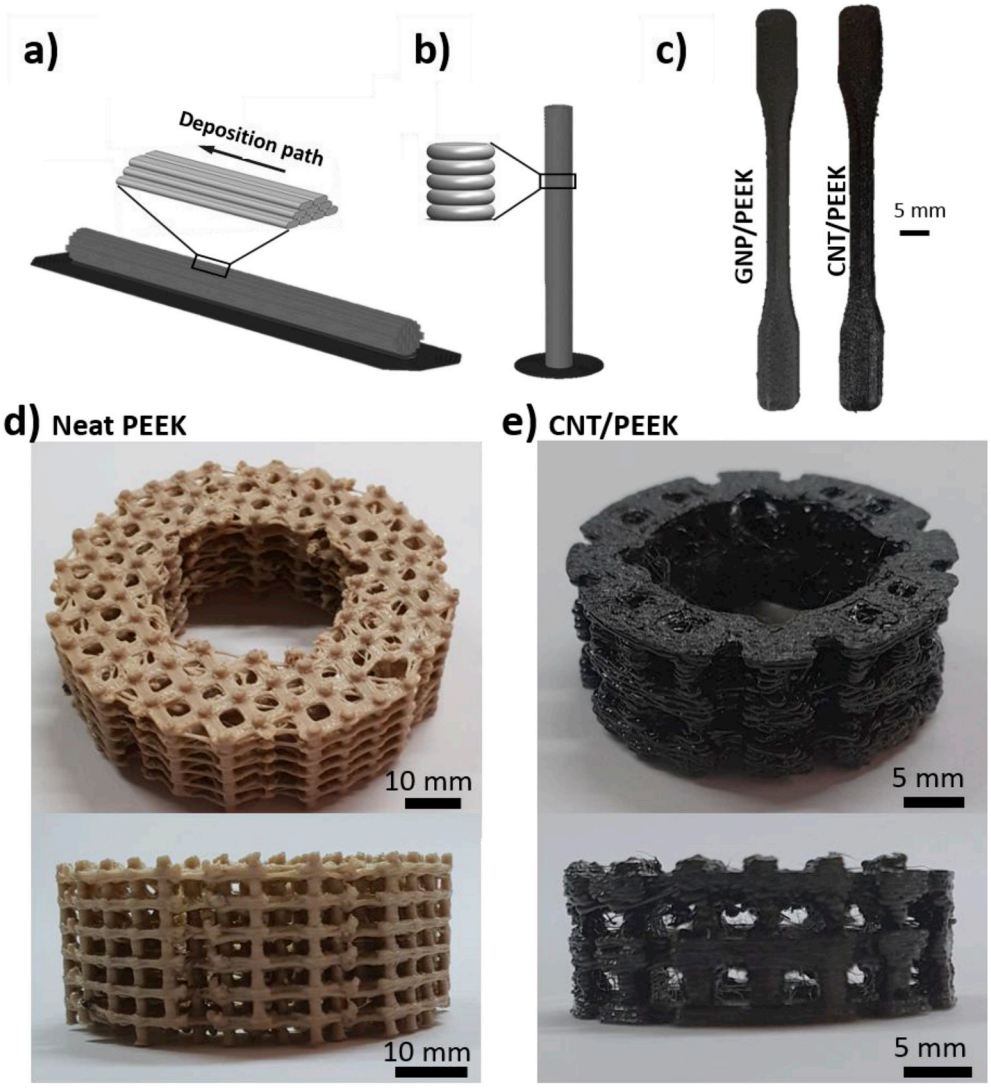

Fig. 1. Additive manufacturing of PEEK and PEEK nanocomposites by FFF. The CTE specimens were fabricated either a) horizontally with 0° raster angle or b) vertically with 90° raster angle. Insert (a,b) shows the magnified view of the deposition path or raster angle. Configuration of the specimen for DMA characterization is similar to that of CTE specimen. c) Horizontally fabricated dogbone specimens were used for tensile testing (also see Fig. S2). Complex 3D printed scaffold geometries of d) neat PEEK and e) CNT/PEEK.

samples underwent a 2nd heating cycle. The melting temperature and heat of fusion data were obtained from the 2nd heating cycle to eliminate the influence of any thermal history and for a better surface contact between the solid sample and the DSC crucible. The degree of crystallinity X_c of the samples was calculated using $X_c = \Delta H_c \times 100/(\Delta H_c^0 w)$, where ΔH_c is the heat of crystallization and ΔH_c^0 is the heat of crystallization of 100% crystalline PEEK (130 J/g [44]), and w is the mass fraction of PEEK in the nanocomposites.

Density of the filament feedstocks and the FFF-samples were determined using a gas (Helium) displacement pycnometry system - AccuPyc II 1340, Micromeritics. Density of FFF-samples made for CTE measurements was measured. Ten repeated measurements were obtained for each sample type. The CTE of the samples was determined using Dilatometer DIL 802 from Bahr Thermoanalyse. The temperature was varied from 30 to 200 °C with a scan rate of 5 °C/min. Cylindrical samples with a diameter of 5 mm and length of 50 mm were analyzed (see Fig. S3). The CTE was estimated from the relationship: $\Delta L/L_0 = \text{CTE}^* \Delta T$, where $\Delta L/L_0$ is the average thermal strain along the length of the sample and ΔT is the change in temperature. Prior to testing, samples were annealed at 200 °C for 3 h to remove thermal history.

Room temperature tensile tests were performed on a (2.5 kN load cell) Zwick-Roell Z005 machine, following ISO 527 standard with a crosshead speed of 1 mm/min. Digital image correlation (DIC) technique was used to obtain the distribution of axial and lateral engineering strains over the gauge length zone of the specimen. We tested only horizontally fabricated samples, with three repeats for statistical purpose. Vertically fabricated samples were not considered as this configuration leads to poor mechanical performance [17]. Prior to testing, samples were annealed at 200 °C for 3 h to remove thermal history. Fractured surfaces of the tensile specimens were examined using Nova NanoSEM to investigate the morphology of the samples and the dispersion quality of CNT and GNP in the PEEK matrix. The samples were mounted on a metal stub and gold sputtered to reduce the charging effects.

Glass transition temperatures (T_g), storage modulus, and tan δ of the PEEK nanocomposites were measured using a dynamic mechanical analyzer (DMA NETZSCH-404 F1 Pegasus®). A bending mode testing was applied during the DMA scans, and the scanning range was from 30 to 250 °C at a heating rate of 3 °C/min and at a frequency of 1 Hz under nitrogen atmosphere. Each sample was tested at least twice to ensure repeatability.

Bulk hardness of the processed samples was analyzed using Vickers's hardness tester (BAREISS-VTEST; Bareiss Prüfgerätebau, Germany) by applying 200-g load (n = 3) with a dwell time of 10 s. The diagonals of the Vickers indents were then measured using an optical microscope to find out the hardness number. To investigate wear performance of the samples, the Fretting wear tests were performed using a ball on a flat configuration (Reciprocating Friction and Wear Monitor TR 281 M

fretting wear testing machine; Bangalore, India). AISI E52100 stainless steel ball with a diameter of 6 mm was used as counter body against fretting of PEEK and PEEK nanocomposites. All the samples were tested at a frequency of 5 Hz and an applied load of 10 N with an amplitude of 100 μm for 10,000 cycles. The wear scar was observed using an optical profilometer (Bruker, contour G T, GTKOX-14-150) to quantify wear volume and wear rate. The wear rate, W (mm^3/Nm) was then calculated using the relationship: $W = \frac{V}{P\lambda S}$, where, V is the wear volume in mm^3, P is the load in N, λ is the amplitude of displacement in m and S is the number of cycles.

3. Results and discussion

3.1. DSC

DSC was performed on filament feedstocks (see, Fig. 2). The melting temperature (T_m), crystallization temperature (T_c), heat of fusion (ΔH_m), heat of crystallization (ΔH_c), and degree of crystallinity (X_c) of neat PEEK and the PEEK nanocomposite filaments were analyzed (see, Table 1). The CNT and GNP reinforced PEEK exhibit a shift in melting and crystallization peaks to a higher temperature compared to the unreinforced PEEK. The T_m is increased by 1 °C and 2 °C with the addition of GNP and CNT, respectively. The T_c shows higher temperature shift than T_m as the T_c increases by 3–4 °C and 5–6 °C with addition of GNP and CNT, respectively. It indicates that the presence of CNT and GNP in PEEK facilitates PEEK crystallization. This is further confirmed by the increase in degree of crystallinity of GNP/PEEK with 3 wt% GNP and CNT/PEEK with 1 wt% CNT. The nano-reinforcements serve as nucleating agents permitting molecular chains of PEEK to pack into a closer arrangement [45,46]. Higher loading of nano-reinforcements (GNP/PEEK with 5 wt% GNP and CNT/PEEK with 3 wt% CNT) exhibit negligible increase in degree of crystallinity. This could be due to the agglomeration of CNT and GNP. Agglomeration reduces the effective contact surface area between the nano-reinforcements and the matrix.

3.2. SEM morphology

Fracture surfaces of tensile specimens were examined to investigate the morphology and dispersion state of the GNP and CNT in PEEK matrix. Figs. 3 and 4 show the SEM images of base PEEK, GNP/PEEK, and CNT/PEEK samples at low (contain several beads) and high magnification, respectively. Fig. 3a shows smooth, brittle-like fracture surface of the base PEEK samples. The interfaces between beads of the base PEEK are not well identifiable, signifying a relatively good adhesion between beads. CNT/PEEK specimen shows surface morphology similar to that of the base PEEK, but with more visible interfaces between beads (Fig. 3c). This indicates that CNT/PEEK sample has more interfacial voids between the beads compared with base PEEK and thus lower interfacial strength. GNP/PEEK sample (see, Figs. 3b and 4b) exhibits a morphology different to those of base PEEK and CNT/PEEK, indicating that the addition of GNP promotes ductility of the nanocomposite. Fig. 4 shows high magnification SEM images of the base PEEK, GNP/PEEK, and CNT/PEEK. It can be seen that CNT and GNP are uniformly dispersed in the PEEK matrix. Moreover, GNP/PEEK composite has large extent of micro and nano-pores. It is worth noting that in all samples, voids with diameters ranging from 50 to 150 μm are observed (see SI, Fig. S4). This is commonly observed in FFF process, arising due to issues, such as non-uniformity of the filament diameter and non-uniform flow of polymer melt.

Table 1
The DSC melting and crystallization data of neat and CNT/GNP reinforced PEEK composites.

	T_m (°C)	T_c (°C)	ΔH_m(J/g)	ΔH_c(J/g)	X_c (%)
PEEK	342	298	29.2	40.8	31
GNP/PEEK (3 wt%)	343	302	28.1	41.5	33
GNP/PEEK (5 wt%)	343	301	27.4	39.7	32
CNT/PEEK (1 wt%)	344	303	28.9	42.4	33
CNT/PEEK (3 wt%)	344	304	27.6	39.0	31

3.3. Density

It can be seen from Table 2 that the density of the filament feedstock slightly increases with increasing CNT and GNP content. This is due to higher density of CNT (1.6 g/cm^3) and GNP (2.267 g/cm^3) than that of the PEEK. All FFF-fabricated nanocomposites exhibit lower density than those of the filament feedstocks. The reduced density of FFF-samples is due to the formation of multiscale voids both within the beads and at the interfaces between the beads during layer-by-layer build-up of the samples. It is interesting to note that horizontally fabricated samples

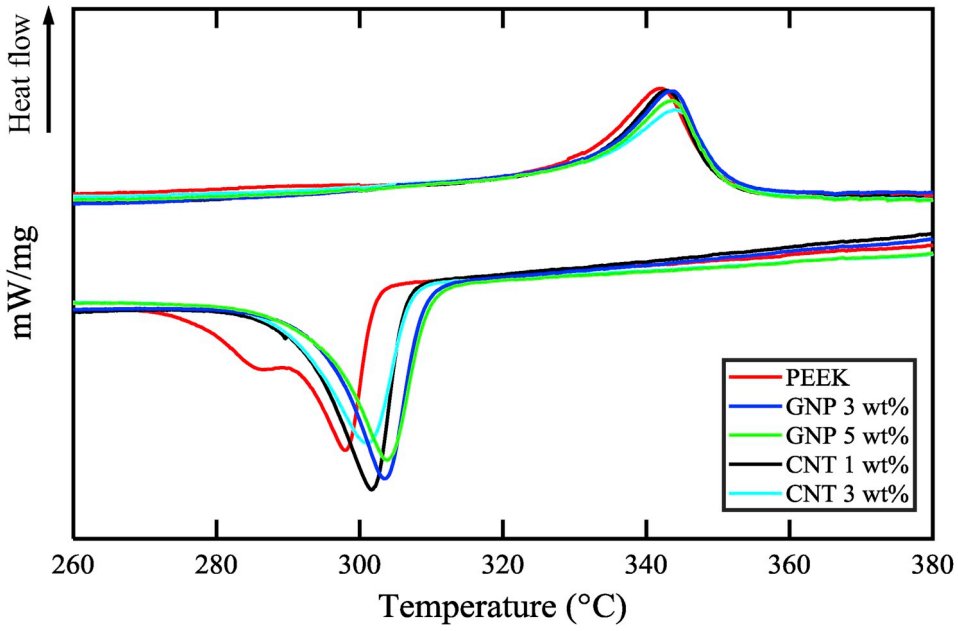

Fig. 2. DSC curves for the neat PEEK and PEEK nanocomposites.

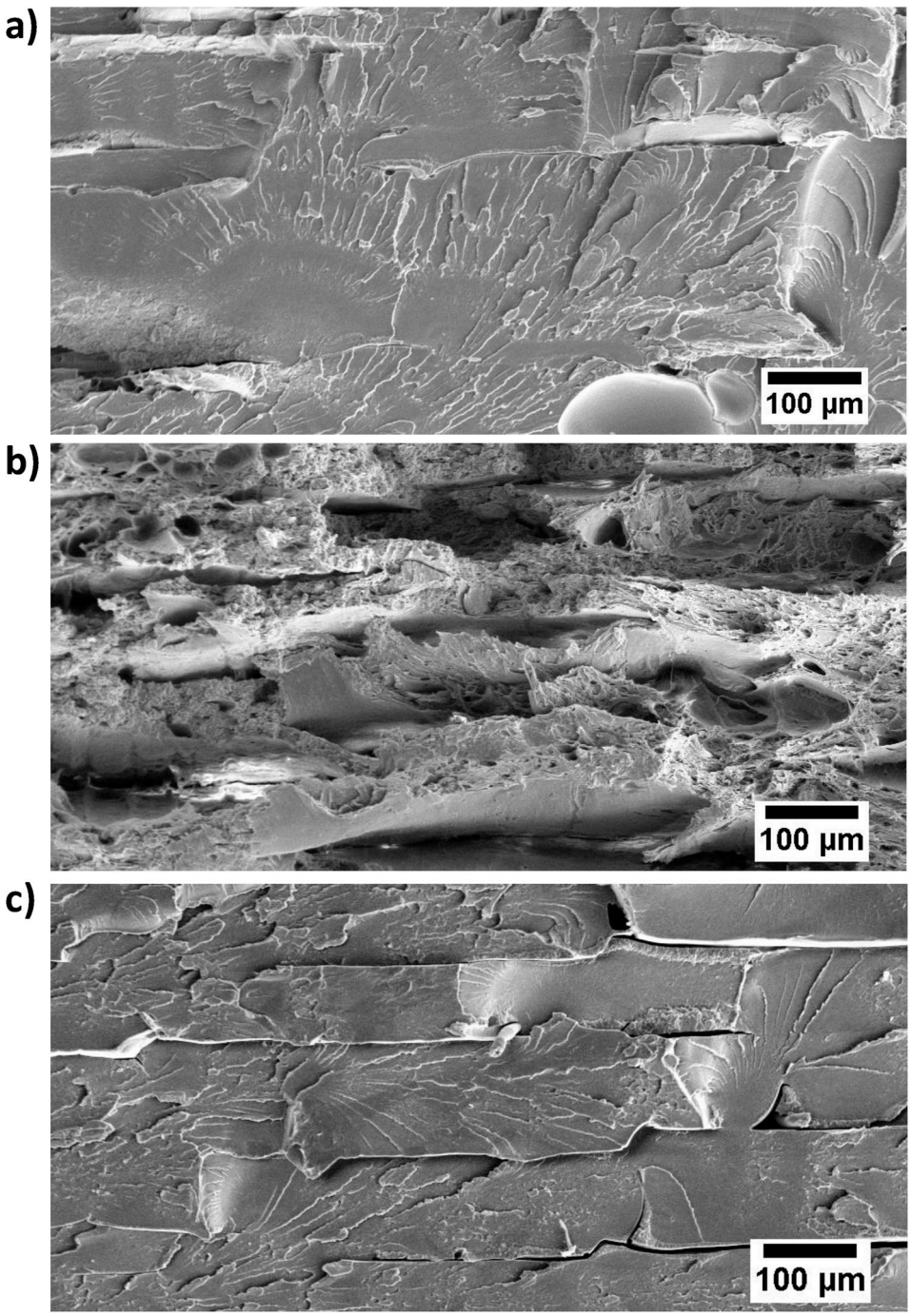

Fig. 3. SEM fracture surface morphology of a) base PEEK, b) GNP/PEEK specimen with 5 wt% GNP and c) CNT/PEEK specimen with 3 wt% CNT. The raster angle and loading direction are normal to the surface.

exhibit lower density than that of vertically fabricated samples. This difference is attributed to the difference in thermal histories of the two configurations, as discussed in our recent work [17].

The polymer melt in vertically fabricated sample is deposited onto a small cross-sectional area, as seen in Fig. 1. Therefore, the deposition time in the $x-y$ plane is very short prior to moving in the z -direction. This allows a good degree of compaction of the sample, resulting in higher density, since the polymer is deposited onto a layer that is still in a molten or partially molten state. The deposition time in the $x-y$ plane of the horizontally fabricated sample is more than that of the vertically fabricated sample. Therefore, it is likely that the bead is deposited on to a solidified preceding layer, resulting in lower degree of compaction of the specimen. Significant difference in density is particularly observed for reinforced nanocomposites. For similar FFF process parameters such as the nozzle movement speed, nozzle temperature and layer height, the mass flow rate of material dispensed through the nozzle for nano-engineered filaments is lower than that for neat PEEK filament. This is due to the increased viscosity and change in flow behavior of fused nanocomposite. Therefore, the extent of interfacial voids between beads of the nanocomposites is higher than that of the base PEEK. This leads to reduced density of the nano-reinforced PEEK composites compared to base PEEK. Moreover, presence of micro and nano-pores within beads are prevalent especially in GNP/PEEK composites, contributing to reduced density of the nano-reinforced PEEK composites.

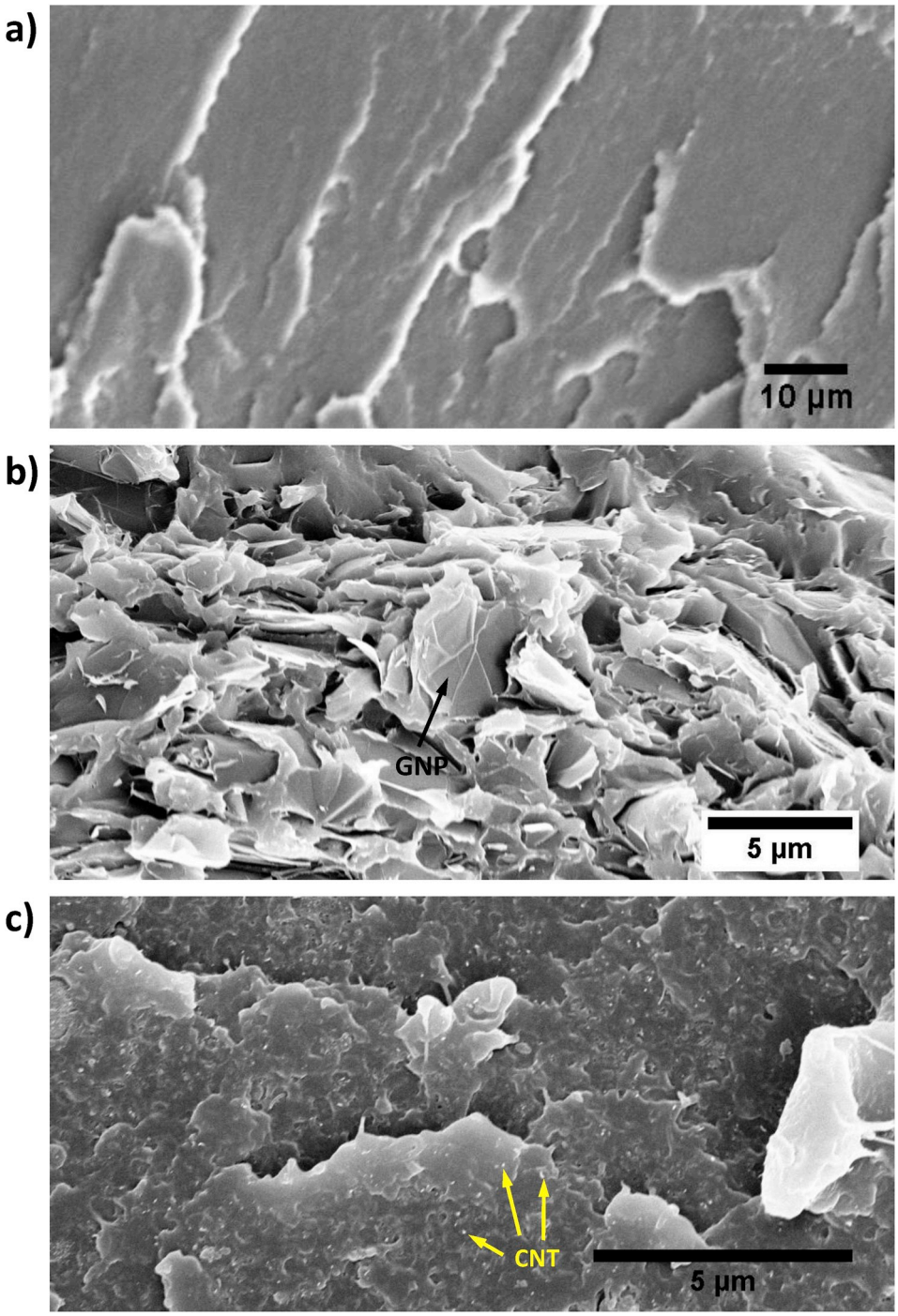

Fig. 4. High magnification micrographs of tensile fracture images of 3D printed a) base PEEK, b) GNP/PEEK composite with 5 wt% GNP, and c) CNT/PEEK composite with 3 wt% CNT. The raster angle and loading direction are normal to the surface.

3.4. CTE of PEEK nanocomposites

The thermal expansion behavior of the samples is influenced by CNT/GNP content, as well as the fabrication configuration. In this study, we measure an average CTE considering thermal expansion only along the longitudinal direction. As seen from Fig. 5, the specimen elongates as the temperature is constantly increased. Two distinct regions, separated by change in slope of strain $\Delta L/L_0$ vs. temperature increase ΔT are observed. This corresponds to the temperature below and above T_g. The CTE was estimated by evaluating the slope of $\Delta L/L_0$ vs. ΔT, below and above T_g. Table 3 summarizes CTE of neat PEEK and PEEK composites with CNT and GNP reinforcements for both horizontal and vertical fabrication configurations. One can see that for temperature below T_g, the CTE of PEEK nanocomposite decreases by 16% and 26% with the addition of 3 wt% GNP and 5 wt% GNP, respectively. Incorporation of CNT into the PEEK matrix reduces the CTE as well but to a lesser extent. The addition of 1 wt% and 3 wt% CNT reduces the CTE of PEEK nanocomposites by 9% and 18%, respectively. The CTE of the nanocomposite above T_g is also evaluated. It should be noted that the mechanical performance of the reinforced PEEK nanocomposites becomes poor in this temperature regime, with a storage modulus of ~10 × lower than that below T_g (see, Fig. 6). The extent of decrease in CTE of the samples with GNP remains the same relative to that below T_g. However, CNT incorporated PEEK specimens above T_g do not exhibit significant CTE changes

Table 2
Density of the filament feedstocks and FFF-fabricated base PEEK and PEEK nanocomposites.

		Density (g/cm^3)
Filament	PEEK	1.30 ± 0.0009
	GNP/PEEK (3 wt%)	1.31 ± 0.0003
	GNP/PEEK (5 wt%)	1.33 ± 0.0014
	CNT/PEEK (1 wt%)	1.30 ± 0.0014
	CNT/PEEK (3 wt%)	1.31 ± 0.0017
PEEK	Fabricated Horizontally	1.28 ± 0.0016
	Fabricated Vertically	1.30 ± 0.0006
GNP/PEEK (3 wt%)	Fabricated Horizontally	1.15 ± 0.0006
	Fabricated Vertically	1.27 ± 0.0009
GNP/PEEK (5 wt%)	Fabricated Horizontally	1.17 ± 0.0005
	Fabricated Vertically	1.24 ± 0.0007
CNT/PEEK (1 wt%)	Fabricated Horizontally	1.21 ± 0.0005
	Fabricated Vertically	1.29 ± 0.0004
CNT/PEEK (3 wt%)	Fabricated Horizontally	1.23 ± 0.0008
	Fabricated Vertically	1.25 ± 0.0006

compared to that of base PEEK. In summary, the horizontally printed nanocomposite samples exhibit lower CTE than the base PEEK, except for CNT reinforced PEEK above T_g. The in-plane CTE of GNP and CNT reinforced PEEK nanocomposites is lower than that of the out-of-plane direction. This is optimally manifested by the horizontally fabricated samples since GNP and CNT tend to orient along the deposition path direction. Insignificant changes in CTE of CNT reinforced PEEK nanocomposites above T_g could be due to different intrinsic thermal expansion property of CNT above T_g. The decrease in CTE with incorporation of GNP and CNT indicates better dimensional stability of the nanocomposites as compared with base PEEK.

The vertically fabricated samples exhibit different trend as compared to horizontally fabricated samples. GNP/PEEK samples show increase in CTE, while CNT/PEEK samples do not exhibit significant changes in CTE, both below and above T_g. The CNT and GNP in vertically fabricated samples are oriented transversely to the specimen's longitudinal direction and thus intrinsically low CTE of CNT and GNP cannot be manifested by the composites. Increased CTE in vertically fabricated GNP/PEEK samples could be due to constraints offered by carbon nanostructures for lateral expansion (as reinforcements are oriented transversely to longitudinal direction) and the resulting Poisson's effect.

3.5. Tensile properties

The tensile performance of base and PEEK nanocomposites is summarized in Table 4. The stress-strain response of the samples are shown in Fig. S5. The Young's modulus of GNP and CNT reinforced PEEK nanocomposites increases with increase in nano-reinforcement content. However, the reinforced nanocomposites exhibit similar tensile strength to that of the base PEEK. The GNP/PEEK nanocomposites exhibit ductile fracture behavior while CNT/PEEK nanocomposites exhibit brittle fracture behavior, as discussed earlier in SEM morphology section. This is reflected in the strain at break and tensile toughness properties of the nanocomposites. Compared to base PEEK, the GNP/PEEK nanocomposites exhibit higher strain at break and toughness properties, while the CNT/PEEK nanocomposites show decreased performance. The Poisson's ratio of the base PEEK and CNT/PEEK nanocomposite samples are similar. However, GNP/PEEK nanocomposite exhibits lower Poisson's ratio. This could be attributed to the greater extent of micro-voids in GNP/PEEK samples, as indicated by SEM image presented in Fig. 4b. It should be noted that the mechanical properties of FFF-parts are influenced by factors such as the bead-bead interfacial strength, nanostructure-PEEK interfacial strength, dispersion state of the nano-reinforcement, interfacial voids between beads and the voids within the beads. The dominating factors that govern the mechanical properties of nano-reinforced FFF samples are the dispersion state of the nano-reinforcement and the interfacial strength between CNT/GNP and PEEK. The macroscopic density measurement presented in Table 2 is influenced by the density of the individual constituents (fiber and matrix), the intra-bead pores, the interfacial voids between beads and the compaction degree during processing. One cannot see a linear relationship between the density (see, Table 2) and the mechanical properties of the horizontally fabricated parts because of these multiple influencing factors.

Table 3
CTE and standard error of base, and CNT and GNP reinforced PEEK nanocomposites. Statistically significant increases/decreases vs. neat PEEK are shown in bracket.

	CTE of Horizontally Fabricated Samples [10^{-6}/K]		CTE of Vertically Fabricated Samples [10^{-6}/K]	
	Below T_g	Above T_g	Below T_g	Above T_g
PEEK	52.17 ± 0.40	128.0 ± 1.25	56.15 ± 0.58	132.4 ± 2.31
GNP/PEEK (3 wt%)	44.04 ± 0.53 (−16%)	105.9 ± 1.29 (−17%)	64.18 ± 0.78 (+14%)	153.4 ± 1.50 (+16%)
GNP/PEEK (5 wt%)	38.63 ± 0.64 (−26%)	92.2 ± 1.91 (−28%)	63.88 ± 0.77 (+14%)	161.8 ± 2.10 (+22%)
CNT/PEEK (1 wt%)	47.30 ± 0.60 (−9%)	135.6 ± 1.64 (+6%)	59.69 ± 0.56 (+6%)	128.0 ± 1.64 (−3%)
CNT/PEEK (3 wt%)	42.70 ± 0.19 (−18%)	124.3 ± 1.47 (−3%)	59.19 ± 0.21 (+5%)	124.9 ± 2.12 (−6%)

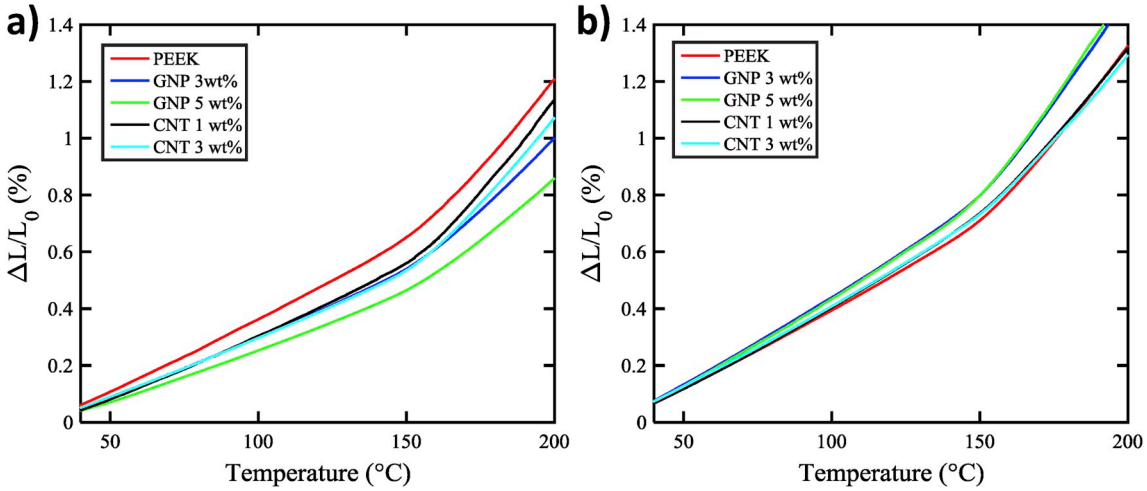

Fig. 5. Thermal expansion behavior of the base and reinforced PEEK composites for a) horizontally fabricated samples and b) vertically fabricated samples.

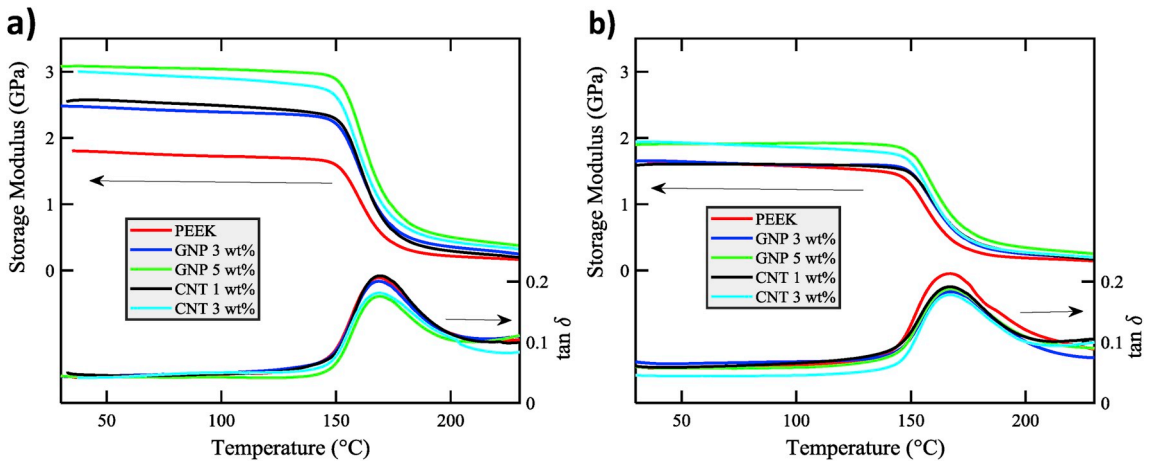

Fig. 6. Storage modulus and tan δ of the base and reinforced PEEK nanocomposites for a) horizontally fabricated samples and b) vertically fabricated samples.

Table 4
Tensile properties of horizontally fabricated samples of base and reinforced PEEK nanocomposites. Statistically significant increases/decreases vs. neat PEEK are shown in bracket.

	PEEK	GNP/PEEK (3 wt%)	GNP/PEEK (5 wt%)	CNT/PEEK (1 wt%)	CNT/PEEK (3 wt%)
Young's Modulus, E_t (GPa)	3.15 ± 0.11	3.68 ± 0.05 (17%)	3.89 ± 0.15 (23%)	3.37 ± 0.04 (7%)	3.77 ± 0.04 (20%)
Tensile strength, σ_m (MPa)	66.2 ± 2.61	66.1 ± 0.96	58.5 ± 3.06 (−12%)	62.5 ± 2.13 (−6%)	63.4 ± 1.02 (−4%)
Tensile elongation, ε_b (%)	3.10 ± 0.32	3.46 ± 0.15 (12%)	3.55 ± 0.17 (15%)	2.66 ± 0.15 (−14%)	2.41 ± 0.21 (−22%)
Toughness ($MJ.m^{-3}$)	1.25 ± 0.19	1.54 ± 0.10 (23%)	1.50 ± 0.16 (20%)	0.98 ± 0.14 (−22%)	0.90 ± 0.12 (−28%)
Poisson's Ratio ν,	0.43 ± 0.01	0.37 ± 0.01 (−14%)	0.32 ± 0.01 (−26%)	0.43 ± 0.01	0.43 ± 0.01

3.6. Dynamic mechanical analysis

DMA analysis for base and nano-reinforced PEEK composites were performed to examine the effect of nano-reinforcement and fabrication configuration on the thermomechanical properties of the PEEK nanocomposites. The storage modulus (E') and tan δ of the PEEK nanocomposites are shown in Fig. 6. In horizontally fabricated samples, incorporation of GNP and CNT into the PEEK matrix increases the storage modulus in the glassy region (below T_g). The higher content of nano-reinforcement results in higher storage modulus. The storage modulus of the samples above T_g reduces drastically, with no significant difference between the base and reinforced PEEK nanocomposites. In contrast, GNP and CNT reinforcements do not significantly influence the storage modulus of vertically fabricated samples in both regimes (below and above T_g). The improved storage modulus of horizontally fabricated samples is due to uniform dispersion of GNP/CNT in the PEEK matrix (see, Fig. 4b and c) which enables efficient stress transfer between the GNP/CNT and PEEK and the improved bead-bead interfacial strength. The vertically fabricated samples do not show significant improvement with GNP/CNT incorporation because the load (in bending mode) in this sample is parallel to multiple weak interfaces between beads. For all the samples, the storage modulus shows a sharp drop at a temperature of 150 °C which indicates the T_g. No significant changes in T_g of both horizontally and vertically fabricated samples are noticed, as seen from the storage modulus onset and peak of tan δ.

3.7. Wear and hardness

Fig. 7a shows the coefficient of friction (COF) as a function of number of cycles for base PEEK and PEEK nanocomposites. COF of the PEEK decreased with the reinforcement of carbon nanostructures from ~0.25 (PEEK) to 0.08 for CNT/PEEK composite at 1 wt % CNT loading and 0.1 for GNP/PEEK composite at 3 wt % GNP loading. The wear volume and wear rate were calculated by scanning the worn surface with the help of an optical profilometer and the results are presented in Table 5. The surface profiles of the scar generated due to wear are shown in Fig. 7b, c and 7d for PEEK, CNT/PEEK and GNP/PEEK respectively. Bulk hardness measured through Vickers's indentation test is presented in Table 5.

The decrease in the COF for PEEK with the addition of carbon nanostructure can be correlated with the hardness. The hardness of CNT/PEEK and GNP/PEEK nanocomposites decreases from ~302 (HV) to ~ 238 and ~279, respectively. The contact areas of the counter body (6 mm dia SS ball) on the samples were calculated using image of the wear scar obtained. Wear rate was minimum in neat PEEK samples (1.23 mm^3/Nm). Carbon nanostructure reinforced PEEK samples, exhibit higher wear rate compared to neat PEEK, i.e., 2.97 and 2.72 mm^3/Nm for CNT/PEEK and GNP/PEEK respectively.

Neat PEEK shows lower wear rate because of higher bulk hardness and higher density, whereas CNT/PEEK and GNP/PEEK nanocomposites showed increased wear rate but lower COF due to their lower hardness and higher multiscale porosity. The increase in surface roughness caused by the CNT/GNP in the FFF printing process and larger extent of micro and nano-pores within the beads and between beads lead to reduced hardness.

4. Summary and conclusions

Carbon nanostructures reinforced PEEK filaments were developed for FFF additive manufacturing and the multifunctional performance of resulting FFF-PEEK nanocomposites were thoroughly investigated. Influence of GNP (3 and 5 wt%) and CNT (1 and 3 wt%) content on the density, CTE, tensile properties, dynamic mechanical properties, wear, friction and hardness characteristics of 3D printed PEEK nanocomposites were investigated. The crystallization temperature and the degree of crystallinity of FFF-PEEK increase with the addition of carbon nanostructures. The print direction influences the extent and distribution of pores and thus the density. For horizontally fabricated samples, the CTE of PEEK nanocomposites significantly decreases by up to 26% and 18% with the addition of 5 wt% GNP and 3 wt% CNT, respectively, indicating a better dimensional stability of the resulting nanocomposite

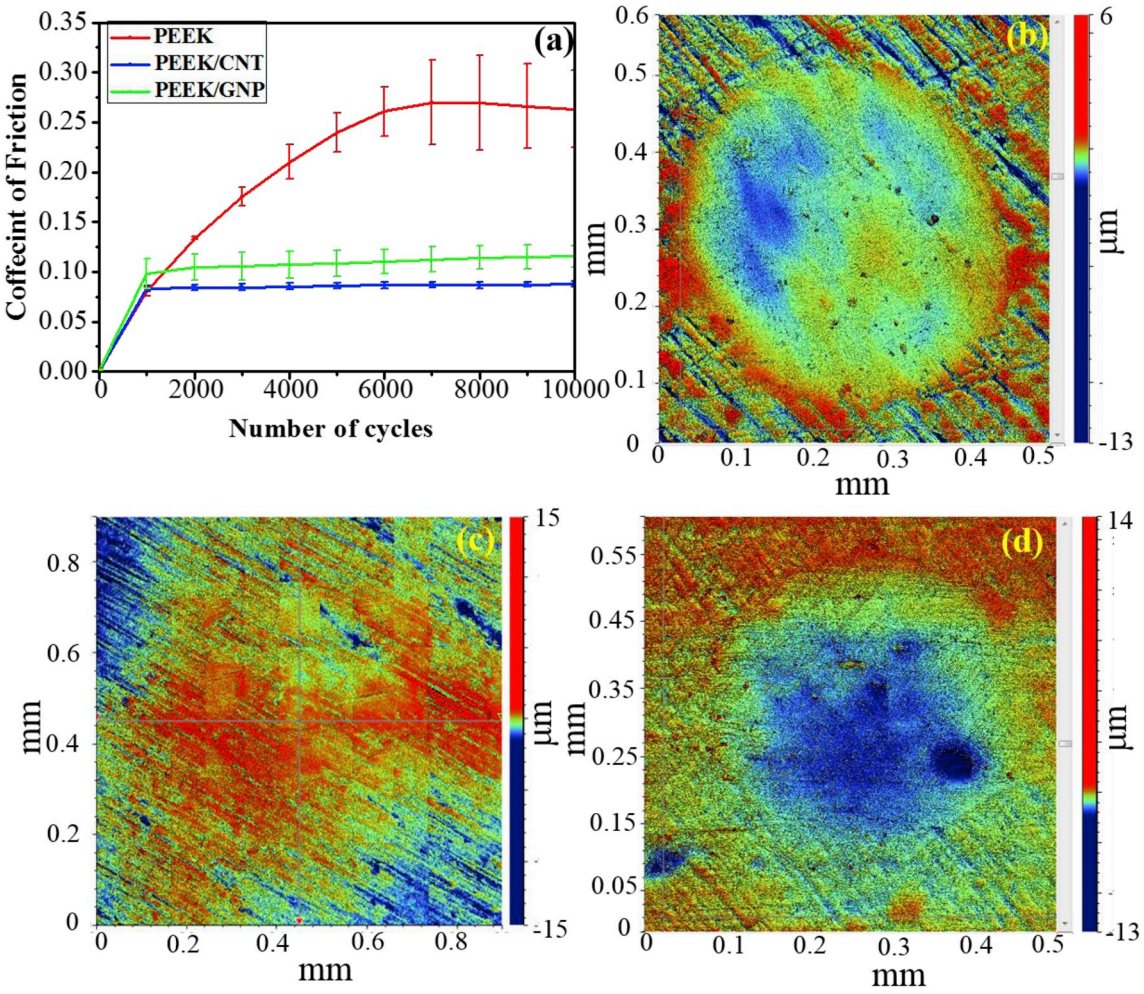

Fig. 7. The COF and 2D images of the wear scar obtained from fretting wear test. (a) COF vs number of cycles, (b) wear scar on PEEK, (c) wear scar on CNT/PEEK (1.0 wt% CNT) nanocomposite and (d) wear scar on GNP/PEEK (3.0 wt% GNP) nanocomposite.

Table 5
The wear characteristics and hardness obtained for the PEEK and PEEK nanocomposites.

Sample	COF	Wear volume (μm^3)	Wear rate (10^{-4}) (mm^3/Nm)	Contact area (mm^2)	Hardness (H_V)
PEEK	0.263 ± 0.038	123,876	1.23	0.126	302.40 ± 22.69
CNT/PEEK (1.0 wt %)	0.087 ± 0.003	297,411	2.97	0.404	238.25 ± 69.65
GNP/PEEK (3.0 wt %)	0.116 ± 0.011	272,877	2.72	0.103	279.63 ± 45.52

structures as compared with neat PEEK.

The tensile modulus of GNP/PEEK and CNT/PEEK nanocomposites increases with increasing nano-reinforcement content. The GNP/PEEK nanocomposites exhibit ductile fracture with concomitant increase in strain at break and toughness relative to neat PEEK. CNT/PEEK nanocomposites exhibit brittle fracture with reduced toughness. Higher micro-voids in GNP/PEEK results in lower Poisson's ratio. Incorporation of GNP and CNT increases the storage modulus in the glassy region due to uniform dispersion of GNP and CNT in the PEEK matrix for horizontally fabricated samples. CNT/PEEK and GNP/PEEK nanocomposites evince higher wear rate but lower COF due to their lower hardness and higher multiscale porosity. All nanocomposite samples examined here formed electrically percolating network and exhibited a minimum electrical conductivity $\sigma = 9.1 \times 10^{-7}$ S/cm (for 1 wt% CNT loading). The multifunctional performance and multiscale characteristics of FFF AM GNP/PEEK and CNT/PEEK nanocomposites demonstrated in this study exhibit their promise for several load bearing and functional applications such as orthopedics, space, oil and gas and automotive.

Acknowledgement

This publication is based upon work supported by the Khalifa University of Science and Technology under Award No. CIRA-2018-128.

Appendix A. Supplementary data

Supplementary data to this article can be found online at https://doi.org/10.1016/j.compositesb.2019.107625.

References

[1] Go J, Schiffres SN, Stevens AG, Hart AJ. Rate limits of additive manufacturing by fused filament fabrication and guidelines for high-throughput system design. Addit Manuf 2017;16:1–11. https://doi.org/10.1016/j.addma.2017.03.007.
[2] Hart AJ, Rao A. How to print a 3D object all at once. Science (80-) 2019;363:1042–3. https://doi.org/10.1126/science.aaw7062.

[3] Kumar S, Wardle BL, Arif MF. Strength and performance enhancement of bonded joints by spatial tailoring of adhesive compliance via 3D printing. ACS Appl Mater Interfaces 2017;9:884–91. https://doi.org/10.1021/acsami.6b13038.

[4] Kumar S, Wardle BL, Arif MF, Ubaid J. Stress reduction of 3D printed compliance-tailored multilayers. Adv Eng Mater 2018;20. https://doi.org/10.1002/adem.201700883. 1700883.

[5] Liljenhjerte J, Upadhyaya P, Kumar S. Hyperelastic strain measurements and constitutive parameters identification of 3D printed soft polymers by image processing. Addit Manuf 2016;11:40–8. https://doi.org/10.1016/j.addma.2016.03.005.

[6] Liljenhjerte J, Kumar S. Pull-out performance of 3D printed composites with embedded fins on the fiber. MRS Proc 2015;1800:mrss15–2135597. https://doi.org/10.1557/opl.2015.645.

[7] de Leon AC, Chen Q, Palaganas NB, Palaganas JO, Manapat J, Advincula RC. High performance polymer nanocomposites for additive manufacturing applications. React Funct Polym 2016;103:141–55. https://doi.org/10.1016/j.reactfunctpolym.2016.04.010.

[8] Panayotov IV, Orti V, Cuisinier F, Yachouh J. Polyetheretherketone (PEEK) for medical applications. J Mater Sci Mater Med 2016;27:118. https://doi.org/10.1007/s10856-016-5731-4.

[9] Rinaldi M, Ghidini T, Cecchini F, Brandao A, Nanni F. Additive layer manufacturing of poly (ether ether ketone) via FDM. Compos B Eng 2018;145:162–72. https://doi.org/10.1016/j.compositesb.2018.03.029.

[10] Yasin S, Shakeel A, Ahmad M, Ahmad A, Iqbal T. Physico-chemical analysis of semi-crystalline PEEK in aliphatic and aromatic solvents. Soft Mater 2019;00:1–7. https://doi.org/10.1080/1539445X.2019.1572622.

[11] Valentan B, Kadivnik Ž, Brajlih T, Anderson A, Drstvenšek I. Processing poly(ether etherketone) on a 3d printer for thermoplastic modelling. Mater Tehnol 2013;47:715–21.

[12] Vaezi M, Yang S. Extrusion-based additive manufacturing of PEEK for biomedical applications. Virtual Phys Prototyp 2015;10:123–35. https://doi.org/10.1080/17452759.2015.1097053.

[13] Wu WZ, Geng P, Zhao J, Zhang Y, Rosen DW, Zhang HB. Manufacture and thermal deformation analysis of semicrystalline polymer polyether ether ketone by 3D printing. Mater Res Innov 2014;18. https://doi.org/10.1179/1432891714Z.000000000898. S5-12-S5-16.

[14] Wu W, Geng P, Li G, Zhao D, Zhang H, Zhao J. Influence of layer thickness and raster angle on the mechanical properties of 3D-printed PEEK and a comparative mechanical study between PEEK and ABS. Materials 2015;8:5834–46. https://doi.org/10.3390/ma8095271.

[15] Cicala G, Latteri A, Del Curto B, Lo Russo A, Recca G, Farè S. Engineering thermoplastics for additive manufacturing: a critical perspective with experimental evidence to support functional applications. J Appl Biomater Funct Mater 2017;15. https://doi.org/10.5301/jabfm.5000343. 0.

[16] Yang C, Tian X, Li D, Cao Y, Zhao F, Shi C. Influence of thermal processing conditions in 3D printing on the crystallinity and mechanical properties of PEEK material. J Mater Process Technol 2017;248:1–7. https://doi.org/10.1016/j.jmatprotec.2017.04.027.

[17] Arif MF, Kumar S, Varadarajan KM, Cantwell WJ. Performance of biocompatible PEEK processed by fused deposition additive manufacturing. Mater Des 2018;146:249–59. https://doi.org/10.1016/j.matdes.2018.03.015.

[18] Berretta S, Evans K, Ghita O. Additive manufacture of PEEK cranial implants: manufacturing considerations versus accuracy and mechanical performance. Mater Des 2018;139:141–52. https://doi.org/10.1016/j.matdes.2017.10.078.

[19] Stepashkin AA, Chukov DI, Senatov FS, Salimon AI, Korsunsky AM, Kaloshkin SD. 3D-printed PEEK-carbon fiber (CF) composites: structure and thermal properties. Compos Sci Technol 2018;164:319–26. https://doi.org/10.1016/j.compscitech.2018.05.032.

[20] Liao G, Li Z, Cheng Y, Xu D, Zhu D, Jiang S, et al. Properties of oriented carbon fiber/polyamide 12 composite parts fabricated by fused deposition modeling. Mater Des 2018;139:283–92. https://doi.org/10.1016/j.matdes.2017.11.027.

[21] Schmitz DP, Ecco LG, Dul S, Pereira ECL, Soares BG, Barra GMO, et al. Electromagnetic interference shielding effectiveness of ABS carbon-based composites manufactured via fused deposition modelling. Mater Today Commun 2018;15:70–80. https://doi.org/10.1016/j.mtcomm.2018.02.034.

[22] Prashantha K, Roger F. Multifunctional properties of 3D printed poly(lactic acid)/graphene nanocomposites by fused deposition modeling. J Macromol Sci Part A 2017;54:24–9. https://doi.org/10.1080/10601325.2017.1250311.

[23] Dul S, Fambri L, Pegoretti A. Fused deposition modelling with ABS–graphene nanocomposites. Compos Part A Appl Sci Manuf 2016;85:181–91. https://doi.org/10.1016/j.compositesa.2016.03.013.

[24] Yu WW, Zhang J, Wu JR, Wang XZ, Deng YH. Incorporation of graphitic nano-filler and poly(lactic acid) in fused deposition modeling. J Appl Polym Sci 2017;134:1–11. https://doi.org/10.1002/app.44703.

[25] Weng Z, Wang J, Senthil T, Wu L. Mechanical and thermal properties of ABS/montmorillonite nanocomposites for fused deposition modeling 3D printing. Mater Des 2016;102:276–83. https://doi.org/10.1016/j.matdes.2016.04.045.

[26] Ryder MA, Lados DA, Iannacchione GS, Peterson AM. Fabrication and properties of novel polymer-metal composites using fused deposition modeling. Compos Sci Technol 2018;158:43–50. https://doi.org/10.1016/j.compscitech.2018.01.049.

[27] Lebedev SM, Gefle OS, Amitov ET, Zhuravlev DV, Berchuk DY, Mikutskiy EA. Mechanical properties of PLA-based composites for fused deposition modeling technology. Int J Adv Manuf Technol 2018;97:511–8. https://doi.org/10.1007/s00170-018-1953-6.

[28] Wu H, Sulkis M, Driver J, Saade-Castillo A, Thompson A, Koo JH. Multi-functional ULTEM^{TM}1010 composite filaments for additive manufacturing using fused filament fabrication (FFF). Addit Manuf 2018. https://doi.org/10.1016/j.addma.2018.10.014.

[29] Goyal R, Tiwari AN, Mulik UP, Negi YS. Novel high performance Al2O3/poly(ether ether ketone) nanocomposites for electronics applications. Compos Sci Technol 2007;67:1802–12. https://doi.org/10.1016/j.compscitech.2006.10.020.

[30] Reddy SK, Kumar S, Varadarajan KM, Marpu PR, Gupta TK, Choosri M. Strain and damage-sensing performance of biocompatible smart CNT/UHMWPE nanocomposites. Mater Sci Eng C 2018;92:957–68. https://doi.org/10.1016/j.msec.2018.07.029.

[31] Gupta TK, Choosri M, Varadarajan KM, Kumar S. Self-sensing and mechanical performance of CNT/GNP/UHMWPE biocompatible nanocomposites. J Mater Sci 2018;53:7939–52. https://doi.org/10.1007/s10853-018-2072-3.

[32] Gupta TK, Kumar S, Khan AZ, Varadarajan KM, Cantwell WJ. Self-sensing performance of MWCNT-low density polyethylene nanocomposites. Mater Res Express 2018;5:015703. https://doi.org/10.1088/2053-1591/aa9f9e.

[33] Arif MF, Kumar S, Gupta TK, Varadarajan KM. Strong linear-piezoresistive-response of carbon nanostructures reinforced hyperelastic polymer nanocomposites. Compos Part A Appl Sci Manuf 2018;113:141–9. https://doi.org/10.1016/j.compositesa.2018.07.021.

[34] Marasso SL, Cocuzza M, Bertana V, Perrucci F, Tommasi A, Ferrero S, et al. PLA conductive filament for 3D printed smart sensing applications. Rapid Prototyp J 2018;24. https://doi.org/10.1108/RPJ-09-2016-0150. 00–00.

[35] Berretta S, Davies R, Shyng YT, Wang Y, Ghita O. Fused Deposition Modelling of high temperature polymers: exploring CNT PEEK composites. Polym Test 2017;63:251–62. https://doi.org/10.1016/j.polymertesting.2017.08.024.

[36] Gonçalves J, Lima P, Krause B, Pötschke P, Lafont U, Gomes J, et al. Electrically conductive polyetheretherketone nanocomposite filaments: from production to fused deposition modeling. Polymers 2018;10:925. https://doi.org/10.3390/polym10080925.

[37] Puértolas JA, Castro M, Morris JA, Ríos R, Ansón-Casaos A. Tribological and mechanical properties of graphene nanoplatelet/PEEK composites. Carbon N Y 2019;141:107–22. https://doi.org/10.1016/j.carbon.2018.09.036.

[38] Kalin M, Zalaznik M, Novak S. Wear and friction behaviour of poly-ether-ether-ketone (PEEK) filled with graphene, WS 2 and CNT nanoparticles. Wear 2015;332–333:855–62. https://doi.org/10.1016/j.wear.2014.12.036.

[39] Malucelli G, Marino F. Abrasion resistance of polymer nanocomposites - a review. In: Adamiak M, editor. Abrasion resist. Mater., IntechOpen; 2012.

[40] Dasari A, Yu Z-Z, Mai Y-W. Wear/scratch damage. 2016. p. 207–26. https://doi.org/10.1007/978-1-4471-6809-6_9.

[41] Zalaznik M, Kalin M, Novak S, Jakša G. Effect of the type, size and concentration of solid lubricants on the tribological properties of the polymer PEEK. Wear 2016;364–365:31–9. https://doi.org/10.1016/j.wear.2016.06.013.

[42] Chao J. Fretting-fatigue induced failure of a connecting rod. Eng Fail Anal 2019;96:186–201. https://doi.org/10.1016/j.engfailanal.2018.10.006.

[43] Koo JH. Polymer nanocomposites: processing, characterization, and applications. second ed. New York: McGraw-Hill; 2019.

[44] Blundell DJ, Osborn BN. The morphology of poly(aryl-ether-ether-ketone). Polymer 1983;24:953–8. https://doi.org/10.1016/0032-3861(83)90144-1.

[45] Kazakova MA, Selyutin AG, Semikolenova NV, Ishchenko AV, Moseenkov SI, Matsko MA, et al. Structure of the in situ produced polyethylene based composites modified with multi-walled carbon nanotubes: in situ synchrotron X-ray diffraction and differential scanning calorimetry study. Compos Sci Technol 2018;167:148–54. https://doi.org/10.1016/j.compscitech.2018.07.046.

[46] Yang B, Wang D, Chen F, Su L-F, Miao J-B, Chen P, et al. Melting and crystallization behaviors of poly(lactic acid) modified with graphene acting as a nucleating agent. J Macromol Sci Part B 2019;58:290–304. https://doi.org/10.1080/00222348.2018.1564222.